Available online at www.sciencedirect.com
ScienceDirect
Ceramics International 37 (2011) 897–902
CERAMICS INTERNATIONAL
www.elsevier.com/locate/ceramint

Enhancement of hydrogen-storage properties of Mg by reactive mechanical grinding with oxide, metallic element(s), and hydride-forming element

Myoung Youp Song [a,*], Sung Nam Kwon [b], Jean-Louis Bobet [c], Hye Ryoung Park [d]

[a] Division of Advanced Materials Engineering, Department of Hydrogen and Fuel Cells, Research Center of Advanced Materials Development, Engineering Research Institute, Chonbuk National University, 664-14 1ga Deogjindong Deogjingu, Jeonju, Jeonbuk, 561-756, Republic of Korea
[b] Department of Hydrogen and Fuel Cells, Chonbuk National University, 664-14 1ga Deogjindong Deogjingu, Jeonju, Jeonbuk, 561-756, Republic of Korea
[c] ICMCB, CNRS [UPR 9048], Université de Bordeaux 1, 33608 Pessac Cedex, France
[d] Faculty of Applied Chemical Engineering, Chonnam National University, 300 Yongbongdong Bukgu, Gwangju, 500-757, Republic of Korea

Received 4 January 2010; received in revised form 23 September 2010; accepted 28 October 2010
Available online 3 December 2010

Abstract

In order to improve the hydrogen-storage properties of magnesium, oxides, metallic element(s) and a hydride-forming element were added to Mg by grinding under a hydrogen atmosphere (reactive mechanical grinding). As the oxides, Fe_2O_3 purchased, Fe_2O_3 prepared by spray conversion, MnO purchased, SiO_2 prepared by spray conversion, and Cr_2O_3 prepared by spray conversion were chosen. As the metallic elements, Ni, Fe, and Mo were selected. In addition, as the hydride-forming element, Ti was selected. Samples with the compositions of Mg–10 wt%oxide, 76.5 wt%Mg–23.5 wt%Ni, 71.5 wt%Mg–23.5 wt%Ni–5wt% Fe_2O_3, 71.5 wt%Mg–23.5 wt%Ni–5 wt%Fe, and Mg–14 wt%Ni–2 wt%Fe–2wt%Ti–2 wt%Mo were prepared. The hydrogen-storage properties and changes in phase and microstructure after the hydriding–dehydriding cycling of the prepared samples were then investigated.

Keywords: H_2-storage properties of Mg; Reactive mechanical grinding; Oxide; Metallic element; Hydride-forming element

1. Introduction

The development of efficient hydrogen storage technology is the main challenge in the forthcoming hydrogen economy, in which energy is stored and transported using hydrogen as an energy carrier for mobile applications (automobiles, aircraft, laptops, etc.). Most of the research on this topic has focused on storing hydrogen safely in lightweight, compact and high capacity systems. There are several hydrogen storage methods currently being investigated: storing hydrogen as a gas, liquid hydrogen storage, the physisorption of hydrogen, and storing it in the form of metal hydrides and complex hydrides, and via chemical reactions [1].

Magnesium is considered as one of the prospective hydrogen storage materials. It has a high hydrogen storage capacity of about 7.6 wt% and is abundant in the earth's crust. However, its hydrogen absorption and desorption rates are very low and its hydrogen absorption and desorption occur at quite high temperatures (at 350–400 °C and over a period of several hours).

Song [2] reviewed the kinetic studies of the hydriding and dehydriding reactions of Mg. Many works do not agree with one another on the rate-controlling step(s) for hydriding or dehydriding reactions of magnesium. However, it is generally accepted that the hydriding and dehydriding reactions of Mg are nucleation-controlled under certain conditions and progress by a mechanism of nucleation and growth, and that the hydriding rates of Mg are controlled by the diffusion of hydrogen through a growing Mg–hydride layer. The hydriding and dehydriding kinetics of Mg can be improved, therefore, by a treatment such as mechanical alloying, which can create defects on the surface and/or in the interior of Mg and reduce the particle sizes of Mg.

The oxides are brittle and, thus, they may be pulverized during mechanical grinding. The added oxides and/or their

* Corresponding author. Tel.: +82 63 270 2379; fax: +82 63 270 2386.
E-mail address: songmy@jbnu.ac.kr (M.Y. Song).

0272-8842/$36.00
doi:10.1016/j.ceramint.2010.11.010

pulverization during mechanical grinding may help the particles of magnesium become finer. Oelerich et al. [3] produced nanocrystalline MgH_2 with the addition of V_2O_5, VN, VC, or high-purity V by high-energy ball milling. The results showed a significant enhancement of the hydrogen reaction kinetics under the chosen experimental conditions only for V_2O_5, VN, and VC, while the influence of high-purity V was negligible. Dehouche et al. [4] investigated the long-term cycling stability as well as the thermal stability of the hydriding–dehydriding properties of nanostructured MgH_2 with 0.2 mol% Cr_2O_3 catalyst addition synthesized by ball milling. High hydriding rates were maintained for at least 17 cycles at 623 K and at least 1000 cycles at 573 K. Barkhordarian et al. [5,6] reported that Nb_2O_5 was superior to all other previously investigated catalysts for the hydrogen sorption reaction of magnesium. They attributed the catalytic effect to electronic exchange reactions with hydrogen molecules, accelerating the gas–solid reaction. Friedrichs et al. [7] and Friedrichs et al. [8] improved the hydrogen sorption kinetics of MgH_2 by milling MgH_2 mechanically with Nb_2O_5 nanoparticles (15 nm). Working as catalysts of reaction products from the Mg–Nb_2O_5 during cycling, and generating gateways of reaction products from the reduction of Nb_2O_5 for further hydrogen diffusion were proposed as two possible reasons for the improvement of the hydrogen sorption kinetics of Mg by them [7]. Aguey-Zinsou et al. [9] improved the (de)hydriding properties of magnesium significantly by mechanical milling MgH_2 with MgO. The MgH_2 particles had an average nanometric size of 0.44 ± 0.3 μm. They reported that the addition of MgO to the grinding medium, which has good lubricant and dispersing properties, allowed the particle size of MgH_2 to be further decreased by reducing the agglomeration and cold welding.

Huot et al. [10] showed that the rapid synthesis of the metal hydride could be achieved by milling at elevated temperature under hydrogen pressure by adding V and graphite to Mg. Liang et al. [11] prepared MgH_2–Tm (Tm = 3d-transition elements Ti, V, Mn, Fe, Ni) nanocomposite powders by intensive mechanical milling. Desorption was most rapid for MgH_2–V, followed by MgH_2–Ti, MgH_2–Fe, MgH_2–Ni and MgH_2–Mn at low temperatures. The composites containing Ti exhibited the most rapid absorption kinetics, followed in order by Mg–V, Mg–Fe, Mg–Mn and Mg–Ni. Li et al. [12] prepared Mg–20 wt% Ni–Y composite by reactive mechanical alloying (RMA). The composite exhibited excellent hydrogen sorption kinetics and did not need activation in the first hydrogen storage process.

Bobet et al. [13] reported that mechanical alloying in H_2 (Reactive Mechanical Grinding) for a short time (2 h) is an effective way to improve the hydrogen-storage properties of both magnesium and Mg + 10 wt% Co, Ni or Fe mixtures. Palade et al. [14] prepared magnesium-rich Mg–Ni–Fe intermetallic compounds and reported that the short time ball milling of the ribbons obtained by melt spinning displayed a better hydrogen desorption kinetics than the long time ball milling of a mixture of MgH_2, Ni and Fe powders. The former preserved a better hydrogen desorption kinetics than the latter.

In this work, in order to enhance the hydrogen-storage properties of magnesium, Mg–oxide and Mg–oxide-metallic element(s) hydrogen storage alloys were prepared by grinding under a hydrogen atmosphere. The hydrogen storage properties and changes in phase and microstructure after hydriding–dehydriding cycling were then investigated.

2. Experimental details

Mg (particle size 297–100 μm, purity 99%, Fluka), Fe_2O_3 (<5 μm, purity 99+%, Aldrich), Fe_2O_3 (36 nm, prepared by spray conversion), Cr_2O_3 (18 nm, prepared by spray conversion), MnO (88–250 μm, purity 99%, Aldrich), SiO_2 (99 nm, prepared by spray conversion), Ni (∼5 μm average, purity 99.9%, CERAC), Fe(<5 μm, purity 99+, Aldrich), Ti (−325 mesh, purity 99.98%, Aldrich), and Mo (1–2 μm, purity 99.9%, Aldrich) were used as starting materials. The preparation of the oxides by spray conversion is explained in detail in reference [15]. A mixture with the desired composition (total weight = 8 g) was introduced into a stainless steel container (with 105 hardened steel balls, total weight = 360 g) sealed hermetically. The sample to ball weight ratio was 1/45. All sample handling was performed in a glove box under Ar in order to prevent oxidation. The mill container with a volume of 250 ml was then filled with high purity hydrogen gas at a pressure of about 10 bar. The reactive mechanical grinding was performed with a disc revolution speed of 250 rpm.

The quantity of absorbed or desorbed hydrogen was measured as a function of time using a volumetric method. A Sievert's type hydriding and dehydriding apparatus comprised of stainless steel pipes is described in Ref. [16]. The hydrogen pressure was maintained at a nearly constant level during the hydriding and dehydriding reactions by dosing or removing an appropriate quantity of hydrogen from or into a standard volume. The variation of the hydrogen pressure in the standard volume portion allows one to calculate the quantity of hydrogen absorbed or desorbed by the sample as a function of time.

Rietveld analysis of the X-ray diffraction (XRD) patterns was carried out using the FullProf program for the dehydrided sample after activation. The microstructures were observed by Scanning Electron Microscope (SEM).

3. Results and discussion

Samples with the compositions Mg–10 wt% oxide (oxide = Fe_2O_3 purchased, Fe_2O_3 prepared by spray conversion, MnO purchased, SiO_2 prepared by spray conversion, and Cr_2O_3 prepared by spray conversion) were prepared by milling for 2 h under high purity hydrogen at a pressure of about 10 bar. We refer to Mg–10 wt%oxide as Mg–10oxide. Fig. 1 shows the weight percentage of absorbed hydrogen, H_a, versus t curves after activation obtained at 593 K and 12 bar H_2 for these samples. The weight percentage of absorbed hydrogen, H_a, is expressed with respect to the sample weight. Mg–10Cr_2O_3 prepared by spray conversion has the highest hydriding rate, followed in order by the Mg–10oxide samples with oxide =

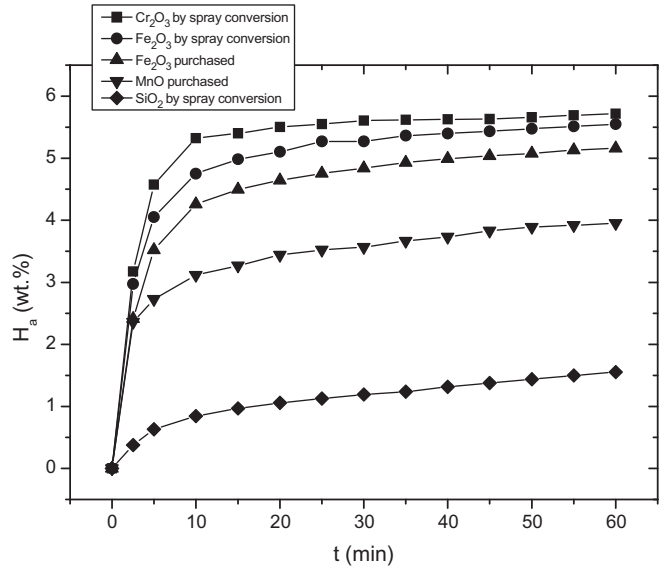

Fig. 1. H_a versus t curves at 593 K and 12 bar H_2 of the activated Mg–10oxide (oxide = Fe_2O_3 purchased, Fe_2O_3 prepared by spray conversion, MnO purchased, SiO_2 prepared by spray conversion, and Cr_2O_3 prepared by spray conversion).

Fe_2O_3 prepared by spray conversion, Fe_2O_3 purchased, MnO purchased, and SiO_2 prepared by spray conversion. Mg–$10Cr_2O_3$ prepared by spray conversion absorbs 5.33 wt% H for 10 min, 5.50 wt% H for 20 min, and 5.72 wt% H for 60 min. Mg–$10Fe_2O_3$ prepared by spray conversion also has a relatively high hydriding rate; It absorbs 4.75 wt% H for 10 min, 5.10 wt% H for 20 min, and 5.55 wt% H for 60 min.

The weight percentage of hydrogen H_d versus t curves obtained at 593 K and 1.0 bar H_2 of the activated Mg–10oxide (oxide = Fe_2O_3 purchased, Fe_2O_3 prepared by spray conversion, MnO purchased, SiO_2 prepared by spray conversion, and

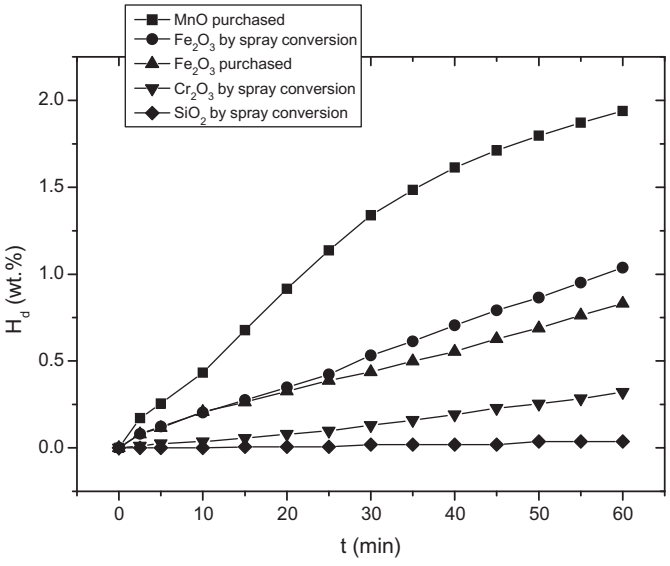

Fig. 2. H_d versus t curve at 593 K and 1.0 bar H_2 of the activated Mg–10oxide (oxide = Fe_2O_3 purchased, Fe_2O_3 prepared by spray conversion, MnO purchased, SiO_2 prepared by spray conversion, and Cr_2O_3 prepared by spray conversion).

Cr_2O_3 prepared by spray conversion) are presented in Fig. 2. The percentage of desorbed hydrogen, H_d, is also expressed with respect to the sample weight. Before obtaining these curves, the sample was hydrided for 1 h under 12 bar H_2 at 593 K. Mg–10MnO purchased has the highest dehydriding rate, followed in order by the samples Mg–10oxide with oxide = Fe_2O_3 prepared by spray conversion, Fe_2O_3 purchased, Cr_2O_3 prepared by spray conversion, and SiO_2 prepared by spray conversion. Mg–10MnO purchased desorbs 0.43 wt% H for 10 min, 0.92 wt% H for 20 min, and 1.94 wt% H for 60 min. Mg–$10Fe_2O_3$ prepared by spray conversion also has a relatively high dehydriding rate; it desorbs 0.20 wt% H for 10 min, 0.35 wt% H for 20 min, and 1.04 wt% H for 60 min.

The above results show that, among the Mg–10oxide samples, Mg–$10Cr_2O_3$ prepared by spray conversion had the highest hydriding rate, followed by Mg–$10Fe_2O_3$ prepared by spray conversion, and the Mg–10MnO purchased had the highest dehydriding rate, followed by Mg–$10Fe_2O_3$ prepared by spray conversion. Based on these results, we chose Fe_2O_3 prepared by spray conversion as the oxide to add to Mg.

We also selected Ni as an element to add, because there have been reports that the addition of Ni to Mg greatly increases its hydriding and dehydriding rates [2,17]. A mechanically alloyed 75 wt% Mg–25 wt% Ni mixture showed high hydriding and dehydriding rates and a large hydrogen storage capacity [17,18]. Yim et al. [19] reported that Mg–23.5 wt% Ni heat-treated after melt spinning had the highest hydrogen-storage capacity and hydriding rate among the samples of Mg–x wt% Ni (x = 13.5, 23.5, and 33.5) prepared by gravity casting, melt spinning, and crystallization heat treatment after melt spinning. We chose the composition 76.5 wt%Mg–23.5 wt%Ni for the preparation of the mixture in this work.

The addition of Fe_2O_3 prepared by spray conversion to Mg with reactive mechanical grinding greatly improved its hydriding rate (Fig. 2). But the preparation of Fe_2O_3 prepared by spray conversion is also a complicated process. We thus used purchased Fe_2O_3 to prepare a mixture with the composition 71.5 wt%Mg–23.5 wt%Ni–5 wt%Fe_2O_3.

Didisheim et al. [20] synthesized the hydride, Mg_2FeH_6, by the reaction of a mixture of Mg and Fe with an atomic ratio of 2:1 with hydrogen in an autoclave under 20–120 bar H_2 at 723–793 K for 2–10 days. They reported that this phase had cubic symmetry with the K_2PtCl_6-type structure and a relatively high hydrogen-storage capacity (5.4 wt%). Fe was chosen as the third additive because it can form Mg_2FeH_6, which has a relatively high hydrogen-storage capacity, by its reaction with Mg and hydrogen. We designed another sample with a similar composition of 71.5 wt%Mg–23.5 wt%Ni–5 wt% Fe.

We prepared 76.5 wt%Mg–23.5 wt%Ni, 71.5 wt%Mg–23.5 wt%Ni–5 wt% Fe_2O_3, and 71.5 wt%Mg–23.5 wt%Ni–5 wt%Fe by reactive mechanical grinding. For the preparation of samples, the mill container was filled with high purity hydrogen gas at a pressure of about 10 bar. Reactive mechanical grinding was performed for 4 h (milling 2 h + refilling with H_2 + milling 2 h).

We refer to 76.5 wt%Mg–23.5 wt%Ni, 71.5 wt%Mg–23.5 wt%Ni–5 wt% Fe_2O_3, and 71.5 wt%Mg–23.5 wt%Ni–5 wt% Fe as Mg–Ni, Mg–Ni–5Fe_2O_3, and Mg–Ni–5Fe, respectively.

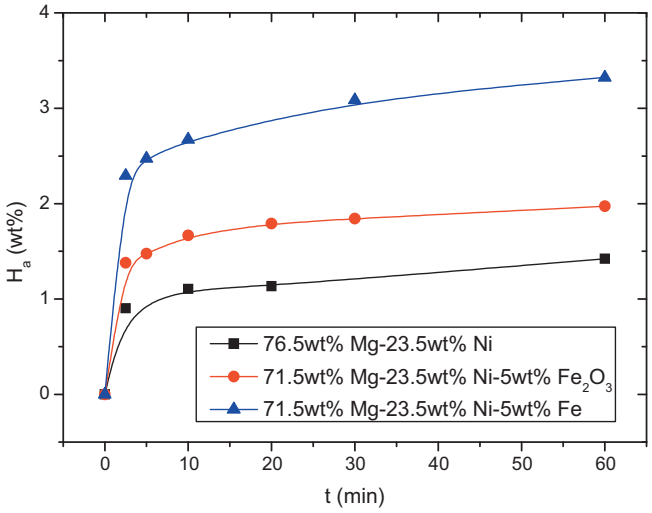

Fig. 3. Variation of the H_a versus t curve after activation (at $n = 3$) at 593 K under 12 bar H_2 with the sample; Mg–Ni, Mg–Ni–5Fe_2O_3, and Mg–Ni–5Fe.

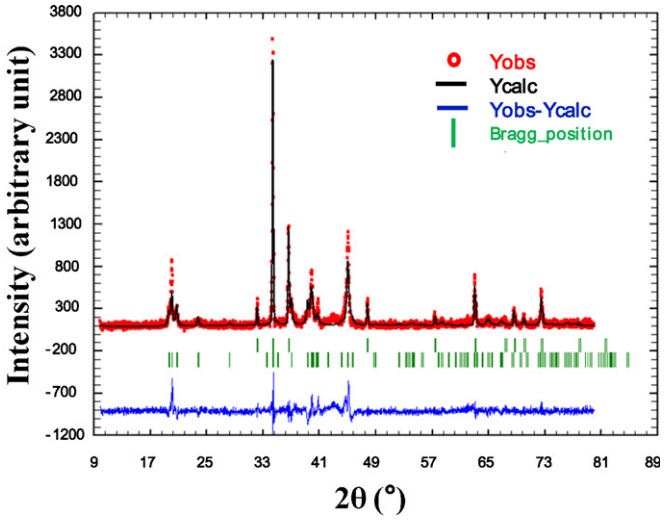

Fig. 5. XRD pattern analyzed by FullProf program of the activated Mg–Ni–5Fe alloy dehydrided in a vacuum at $n = 5$.

Fig. 3 shows the variation of the weight percentage of absorbed hydrogen H_a versus t curve after activation (at $n = 3$) with the sample at 593 K under 12 bar H_2 for the samples Mg–Ni, Mg–Ni–5Fe_2O_3, and Mg–Ni–5Fe. Before obtaining these curves, measurements of the dehydriding curves were performed, and then the samples were dehydrided for 2 h in a vacuum at 623 K. Mg–Ni–5Fe has the highest hydriding rate (0.494 wt% H/min for 5 min) and the largest value of H_a after 60 min (3.32 wt%). The hydriding rate and H_a value after 60 min decrease in the order of Mg–Ni–5Fe_2O_3 and Mg–Ni.

The variation of the weight percentage of desorbed hydrogen H_d versus t curve after activation (at $n = 3$) with the sample at 593 K under 1.0 bar H_2 was studied for the samples Mg–Ni, Mg–Ni–5Fe_2O_3, and Mg–Ni–5Fe. Before obtaining these curves, the sample was hydrided for 1 h under 12 bar H_2 at 593 K. Mg–Ni–5Fe had the highest dehydriding rate (0.330 wt% H/min for 5 min) and the dehydriding rate decreased in the order of Mg–Ni–5Fe_2O_3 and Mg–Ni. In the samples Mg–Ni, Mg–Ni–5Fe_2O_3, and Mg–Ni–5Fe, the hydriding and dehydriding reactions of Mg_2Ni and Mg phases occur under the hydriding and dehydriding conditions used in this work.

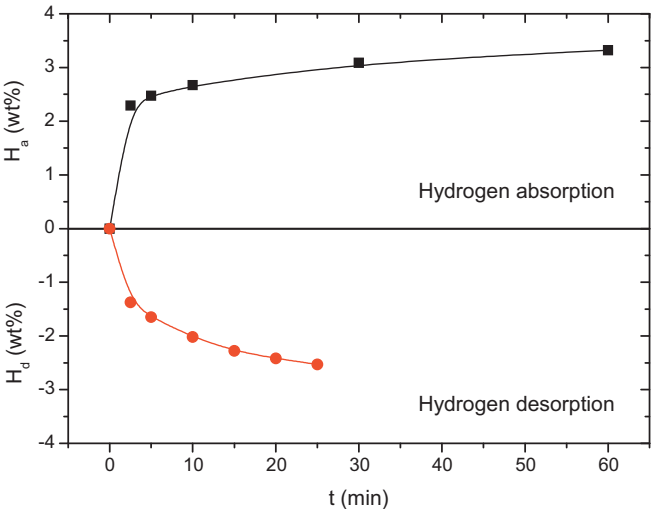

Fig. 4. Hydriding curve under 12 bar H_2 and dehydriding curve under 1.0 bar H_2 for the sample Mg–Ni–5Fe after activation (at $n = 3$) at 593 K.

The hydriding curve under 12 bar H_2 and the dehydriding curve under 1.0 bar H_2 for the sample Mg–Ni–5Fe after activation (at $n = 3$) at 593 K are presented in Fig. 4. Under these hydriding and dehydriding conditions, the hydriding rate is much higher than the dehydriding rate. The hydriding rate for 5 min is 0.494 wt% H/min, and the dehydriding rate for 5 min is 0.330 wt% H/min. This sample Mg–Ni–5Fe absorbs 2.47 wt% H for 5 min, 2.67 wt% H for 10 min, and 3.32 wt% H for 60 min. It desorbs 1.65 wt% H for 5 min, 2.02 wt% H for 10 min, and 2.42 wt% H for 60 min.

Fig. 5 shows the XRD pattern of the activated Mg–Ni–5Fe alloy dehydrided in a vacuum at $n = 5$. The sample contains Mg, Mg_2Ni, MgO, and Fe. The bars indicating the diffraction angles are drawn downward in the figure by the order of the Mg and Mg_2Ni phases. Table 1 shows the results of the analysis of the XRD pattern by FullProf program of the activated Mg–Ni–5Fe alloy dehydrided in a vacuum at $n = 5$. MgO and Fe are not considered for refinement because they are present as traces only. The R factors measuring the agreement between the reflection intensities (Bragg R-factor) or structure factors (Rf-factor) calculated from a crystallographic model and those measured experimentally are quite small. The weight percentages calculated by Full Proof program of Mg and Mg_2Ni are 55.52 and 44.48, respectively.

Table 1
Results of the analysis of the XRD pattern by FullProf program of the activated Mg–Ni–5Fe alloy dehydrided in a vacuum at $n = 5$.

Phase	Bragg R-factor	Rf-factor	Fraction (wt%)
Mg	5.66	4.81	55.52 (1.21)
Mg_2Ni	25.0	17.6	44.48 (0.94)

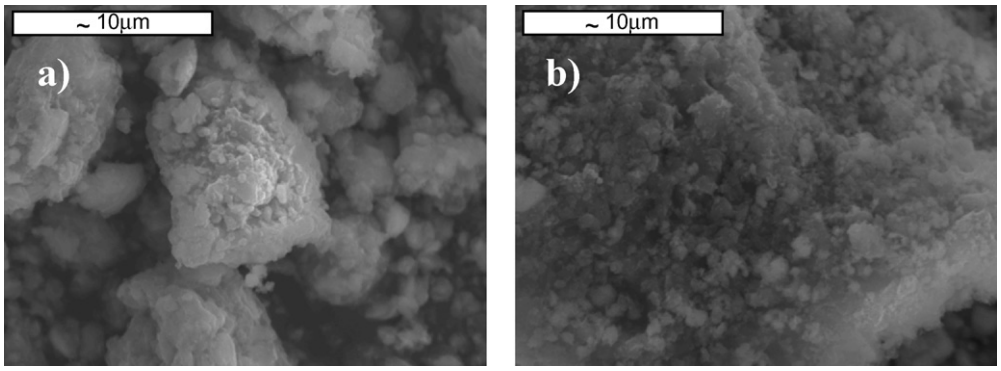

Fig. 6. Microstructures of the Mg–Ni–5Fe alloy (a) after reactive mechanical grinding and (b) after hydriding–dehydriding cycling (at $n = 3$).

The microstructures of the Mg–Ni–5Fe alloy after reactive mechanical grinding and after hydriding–dehydriding cycling (at $n = 3$) are exhibited in Fig. 6. The sample after hydriding–dehydriding cycling has finer particles than that after reactive mechanical grinding. The expansion and contraction of the hydride-forming materials (Mg and Mg_2Ni) with the hydriding and dehydriding reactions is considered to create defects and cracks which can lead to the fragmentation of the particles.

To develop an alloy with better hydrogen-storage properties than the Mg–Ni–5Fe alloy, a sample with the composition of Mg–14 wt%Ni–2 wt%Fe–2 wt%Ti–2 wt%Mo was prepared by milling for 6 h under approximately 12 bar H_2. During milling hydrogen was refilled every one hour. Ti is expected to form titanium hydride, which is brittle and may help the mixture pulverized during grinding. The Mg–14 wt%Ni–2 wt%Fe–2 wt%Ti–2 wt%Mo sample is named as Mg–14Ni–2Fe–2Ti–2Mo. Liang et al. [11] prepared MgH_2–Tm (Tm = 3d-transition elements Ti, V, Mn, Fe, Ni) nanocomposite powders by intensive mechanical milling. The composites containing Ti exhibited the most rapid absorption kinetics, followed in order by Mg–V, Mg–Fe, Mg–Mn and Mg–Ni.

The variation of the H_a versus t curve with the number of cycles for the as-milled Mg–14Ni–2Fe–2Ti–2Mo at 573 K under 12 bar H_2 is presented in Fig. 7. The activation is completed after $n = 3$. At $n = 3$, the values of H_a are 4.35 wt% after 5 min, 4.47 wt% for 10 min, and 4.61 wt% after 60 min. During hydriding the sample, hydriding reactions of Mg and Mg_2Ni phases occur under these experimental conditions.

Fig. 8 shows the hydriding curve under 12 bar H_2 and the dehydriding curve under 1.0 bar H_2 for the sample Mg–14Ni–2Fe–2Ti–2Mo after activation (at $n = 3$) at 573 K. This alloy absorbs 4.35 wt% H for 5 min, 4.47 wt% H for 10 min, and 4.61 wt% H for 60 min. This alloy desorbs 0.96 wt% H for 5 min, 2.00 wt% H for 10 min, and 4.58 wt% H for 60 min. Mg–14Ni–2Fe–2Ti–2Mo has higher hydriding and dehydriding rates than any of the other samples prepared in this work. The increase in the Mg content and the addition of transition metals are considered to increase the hydriding and dehydriding rates. The dehydriding curve has a shape exhibiting two stages; the first one with a relatively high dehydriding rate and the second one with a lower dehydriding rate. It is considered that, in the first stage, the Mg_2Ni hydride and Mg hydride with smaller particle sizes decompose and that, in the second stage, the dehydriding reaction of Mg hydride with larger particle sizes occurs.

An enlarged hydriding curve, after about 1.2 min, at 573 K under 12 bar H_2, for the sample Mg–14Ni–2Fe–2Ti–2Mo after

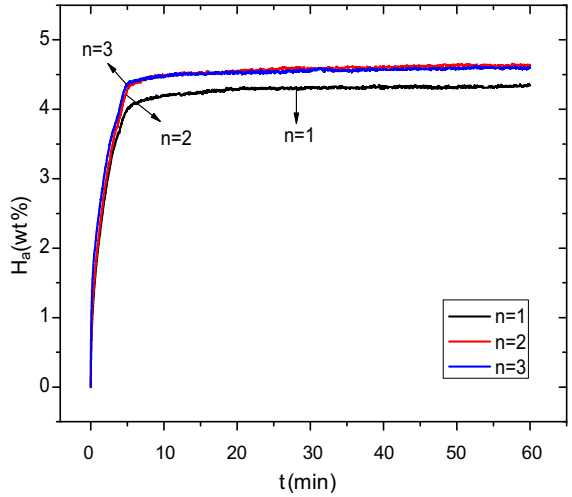

Fig. 7. Variation of the H_a versus t curve with the number of cycles for the as-milled Mg–14Ni–2Fe–2Ti–2Mo at 573 K under 12 bar H_2.

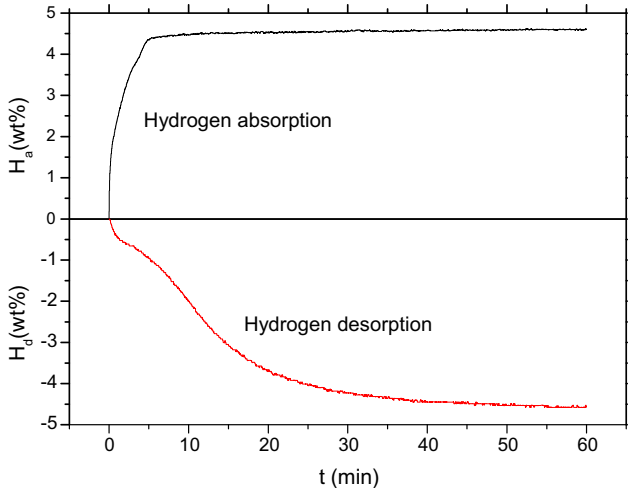

Fig. 8. Hydriding curve under 12 bar H_2 and dehydriding curve under 1.0 bar H_2 for the sample Mg–14Ni–2Fe–2Ti–2Mo after activation (at $n = 3$) at 573 K.

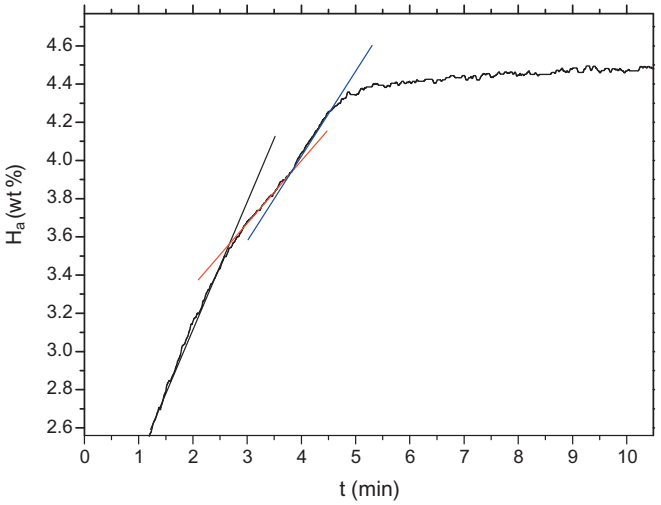

Fig. 9. Enlarged hydriding curve, after about 1.2 min, at 573 K under 12 bar H_2, for the sample Mg–14Ni–2Fe–2Ti–2Mo after activation (at $n = 3$).

activation (at $n = 3$) is shown in Fig. 9. This figure shows that the hydriding curve also has a shape exhibiting two stages, the second one appearing after about 4 min. It is considered that, in the first stage, Mg_2Ni and Mg with smaller particle sizes absorb hydrogen and that, in the second stage, the hydriding reaction of Mg with larger particle sizes occurs.

The reactive mechanical grinding of Mg with oxides, Ni, Fe, Ti and/or Mo and hydriding–dehydriding cycling are considered to increase the hydriding and dehydriding rates by facilitating nucleation (by creating defects on the surface of the Mg particles and by the additive) and by reducing the particle size of Mg and, thus, by shortening the diffusion distances of the hydrogen atoms. The Mg_2Ni phase formed by the reaction of Mg with Ni is also considered to contribute to the increase of the hydriding and dehydriding rates. On the other hand, maintaining the mixture at a relatively high temperature (e.g. 593 K) during hydriding–dehydriding cycling causes the particles to coalesce by sintering, leading to an increase of the particle size. This will bring about a decrease in the hydriding and dehydriding rates.

4. Conclusions

Among the Mg–10oxide samples, Mg–10Cr_2O_3 prepared by spray conversion had the highest hydriding rate and Mg–10MnO purchased had the highest dehydriding rate. Among the samples Mg–Ni, Mg–Ni–5Fe_2O_3, and Mg–Ni–5Fe, the latter had the highest hydriding rate (0.494 wt% H/min for 5 min at 593 K under 12 bar H_2) and the highest dehydriding rate (0.330 wt% H/min for 5 min at 593 K under 1.0 bar H_2). For the activated Mg–Ni–5Fe alloy dehydrided in a vacuum at $n = 5$, the weight percentages calculated by FullProf program of Mg and Mg_2Ni were 55.52 and 44.48, respectively. The reactive mechanical grinding of Mg with Ni, Fe_2O_3 or Fe, and hydriding–dehydriding cycling are considered to increase the hydriding and dehydriding rates by facilitating nucleation and by reducing the particle size of Mg. The Mg_2Ni phase formed by the reaction of Mg with Ni is also believed to contribute to the increase of the hydriding and dehydriding rates. Mg–14Ni–2Fe–2Ti–2Mo, with higher hydriding and dehydriding rates than any of the other samples prepared in this work, absorbed 4.61 wt% H at 573 K 12 bar H_2, and desorbed 4.58 wt% H at 573 K 1.0 bar H_2 for 60 min.

Acknowledgements

This research was performed for the Hydrogen Energy R&D Center, one of the 21st Century Frontier R&D Program, funded by the Ministry of Science and Technology, Republic of Korea. This paper was supported by the selection of research-oriented professor (Myoung Youp Song) of Chonbuk National University in 2009.

References

[1] A. Züttel, Mater. Today 6 (9) (2003) 24.
[2] M.Y. Song, J. Mater. Sci. 30 (1995) 1343.
[3] W. Oelerich, T. Klassen, R. Bormann, J. Alloy Compd. 322 (2001) L5.
[4] Z. Dehouche, T. Klassen, W. Oelerich, J. Goyette, T.K. Bose, R. Schulz, J. Alloy Compd. 347 (2002) 319.
[5] G. Barkhordarian, T. Klassen, R. Bormann, Scripta Mater. 49 (2003) 213.
[6] G. Barkhordarian, T. Klassen, R. Bormann, J. Alloy Compd. 407 (1–2) (2006) 249.
[7] O. Friedrichs, T. Klassen, J.C. Sánchez-López, R. Bormann, A. Fernández, Scripta Mater. 54 (7) (2006) 1293.
[8] O. Friedrichs, F. Aguey-Zinsou, J.R. Ares Fernández, J.C. Sánchez-López, A. Justo, T. Klassen, R. Bormann, A. Fernández, Acta Mater. 54 (1) (2006) 105.
[9] K.-F. Aguey-Zinsou, J.R. Ares Fernandez, T. Klassen, R. Bormann, Mater. Res. Bull. 41 (6) (2006) 1118.
[10] J. Huot, M.-L. Tremblay, R. Schulz, J Alloy Compd. 356–357 (2003) 603.
[11] G. Liang, J. Huot, S. Boily, A. Van Neste, R. Schulz, J Alloy Compd. 292 (1–2) (1999) 247.
[12] Z. Li, X. Liu, L. Jiang, S. Wang, Int. J. Hydrogen Energy 32 (12) (2007) 1869.
[13] J.-L. Bobet, E. Akiba, Y. Nakamura, B. Darriet, Int. J. Hydrogen Energy 25 (2000) 987.
[14] P. Palade, S. Sartori, A. Maddalena, G. Principi, S. Lo Russo, M. Lazarescu, G. Schinteie, V. Kuncser, G. Filoti, J. Alloy Compd. 415 (1–2) (2006) 170.
[15] M.Y. Song, S.H. Hong, I.H. Kwon, S.N. Kwon, C.G. Park, J.S. Bae, J. Alloy Compd. 398 (1–2) (2005) 283.
[16] M.Y. Song, S.H. Baek, J.L. Bobet, S.H. Hong, Int. J. Hydrogen Energy 35 (2010) 10366.
[17] M.Y. Song, E.I. Ivanov, B. Darriet, M. Pezat, P. Hagenmuller, J. Less-Common Met. 131 (1987) 71.
[18] M.Y. Song, Int. J. Hydrogen Energy 20 (3) (1995) 221.
[19] C.D. Yim, B.S. You, Y.S. Na, J.S. Bae, Catal. Today 120 (2007) 276.
[20] J.J. Didisheim, P. Zolliker, K. Yvon, P. Fischer, J. Schefer, M. Gubelmann, A.F. Williams, Inorg. Chem. 23 (1984) 1953.